

PAPER • OPEN ACCESS

## Current interruption performance of ultrahigh-pressure nitrogen arc

To cite this article: Fahim Abid *et al* 2020 *J. Phys. D: Appl. Phys.* **53** 185503

View the [article online](#) for updates and enhancements.



**IOP | ebooks™**

Bringing together innovative digital publishing with leading authors from the global scientific community.

Start exploring the collection—download the first chapter of every title for free.

# Current interruption performance of ultrahigh-pressure nitrogen arc

Fahim Abid<sup>1</sup> , Kaveh Niayesh<sup>1</sup>, Camilla Espedal<sup>2</sup> and Nina Støa-Aanensen<sup>2</sup>

<sup>1</sup> Department of Electric Power Engineering, Norwegian University of Science and Technology, Trondheim, Norway

<sup>2</sup> SINTEF Energy Research, Trondheim, Norway

E-mail: [fahim.abid@ntnu.no](mailto:fahim.abid@ntnu.no)

Received 11 December 2019, revised 15 January 2020

Accepted for publication 6 February 2020

Published 03 March 2020



## Abstract

In this paper, the influence of gas filling pressure on the current interruption performance of different switch configurations with electric arcs burning in nitrogen has been experimentally investigated. A synthetic circuit generating a current of 130 A at 190 Hz is used and the initial rate of rise of recovery voltage just after current zero is varied from 9.8 V/ $\mu$ s to 84.9 V/ $\mu$ s. To evaluate the effect of forced gas flow on current interruption performance, three different test arrangements are investigated: a simple contact configuration with a free-burning arc, a contact and a cylindrical nozzle setup (tube-constricted arc), and finally a self-blast arrangement where the arc is cooled by a gas flow near current zero. In each arrangement, three different filling pressures are mainly studied: 1, 20, and 40 bar, the latter being in the supercritical region. In all cases, the interelectrode gap is fixed at 50 mm. It is observed that the interruption performance deteriorates with increased filling pressure in the absence of forced gas flow. A higher post-arc current is observed for the arcs burning at high filling pressures (i.e. 20 and 40 bar) compared to at atmospheric pressure in cases with no or little forced cooling. On the other hand, a forced gas flow near the current zero reduces the post-arc current and improves the interruption performance also at high filling pressures. Little effect of the supercritical state on the interruption performance of nitrogen is observed. Under the above-mentioned test conditions, the majority of the failures at high filling pressure are observed to be of thermal re-ignition type.

Keywords: supercritical fluid, arc discharge, current interruption

(Some figures may appear in colour only in the online journal)

## 1. Introduction

An increasing number of offshore wind farms as well as other activities located far off the coast lead to the need for offshore substations. To avoid the large costs associated with platforms and floaters, power switching equipment and other components of such an offshore substation can be placed on the seabed and controlled remotely [1]. The conventional solution is to use thick-walled pressure-proof vessels to provide an environment for the power components like that of onshore

installations [2]. Power cable feed-throughs or penetrators from the high-pressure water environment and into the low gas pressure inside the vessel are also required. These features add substantial technical complexity and cost, in particular at large sea depths. However, filling the interrupting chamber of the switchgear with high-pressure gas will reduce the differential pressure over the metal enclosure. The interruption chamber can be filled gradually as the switchgear is lowered and finally reaching the same pressure as is present at the seabed. Reducing the differential pressure will reduce the cost of the encapsulations and feed-throughs.

If the temperature and pressure of a gas exceed a critical point, it enters into the supercritical (SC) region. The physical properties of an SC fluid are somewhere between gas and liquid. For example, an SC fluid has a high density, while the



Original content from this work may be used under the terms of the [Creative Commons Attribution 4.0 licence](https://creativecommons.org/licenses/by/4.0/). Any further distribution of this work must maintain attribution to the author(s) and the title of the work, journal citation and DOI.

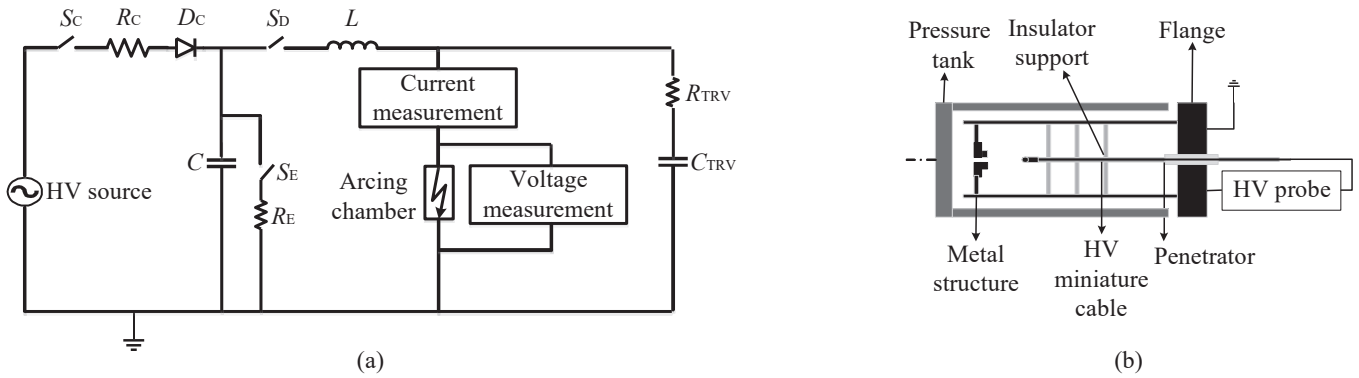


**Figure 1.** Test circuit. (a) Electrical setup, (b) schematics of the arcing chamber (pressure vessel).

viscosity is low like a gas. Other important properties of an SC fluid include high diffusivity, high heat conductivity, high heat capacity, and an absence of vapor bubbles. In power switching applications, the switchgear must fulfill extreme demands, such as high dielectric strength during off time, low resistance during on time, high current handling capability, high voltage rating, fast switching time, fast recovery after switching, and long lifetime. An SC fluid is believed to have favorable properties in this regard [3].

To study SC arc discharges, nitrogen ( $N_2$ ) is chosen due to its environmentally benign nature, good insulation strength and low critical pressure. The critical point of  $N_2$  is at 126 K and 33.5 bar [4]. Thus, at room temperature when  $N_2$  is pressurized to more than 33.5 bar, it enters into the SC region. Arc discharges at extremely high gas pressures have rarely been investigated in the past. Among the works published, some focus on underwater welding applications [5, 6] whereas some focus on the fundamental understanding of electrical discharges inside SC carbon dioxide or SC  $N_2$  [7–11]. These fundamental works investigate very small energy discharges in the range of millijoules with interelectrode gap distances in the millimeter range. However, for circuit breaker applications, the energy deposition in the arc are normally up to hundreds of kilojoules. Recently, efforts have been made to experimentally investigate the characteristics of high energy  $N_2$  arc discharges at different filling pressures, up to 98 bar [12]. The free-burning arc voltage is reported to increase with filling pressure of  $N_2$  without any abrupt change during the transition from gas to SC state [12]. The arc radius decreases as the filling pressure increases [13, 14].

To the author's knowledge, there is no experimental work published regarding current interruption in ultrahigh-pressure  $N_2$  for circuit breaker applications. To be able to interrupt the current, the breaker must successfully handle both the thermal and dielectric phases [15]. A finite post-arc current is often observed in the contact gap just after CZ due to the remaining electrical conductivity and the voltage stress due to transient recovery voltage (TRV) [15]. If the energy deposited in the post-arc channel due to the post-arc current is high enough, a thermal re-ignition may occur. Thermal re-ignition occurs almost immediately (up to some tens of microseconds) after CZ [16]. Re-ignition is reported to be greatly dependent on

the initial rate of rise of recovery voltage (IRRRV) and the steepness of the current ( $di/dt$ ) before CZ [15]. Moreover, even after successfully passing the thermal phase, a dielectric restrike may occur if the TRV exceeds the dielectric strength of the switching gap. A dielectric restrike typically occurs several hundred microseconds after CZ when the TRV reaches its peak value [17].

In this paper, the current interruption performance of  $N_2$  as a function of filling pressure is reported. To evaluate the effect of forced gas flow on the current interruption performance, three different test arrangements are adopted. First, a free-burning arc (without any forced gas flow) at different filling pressure is studied. Afterward, to explore the effect of tube-constriction on the arc, the arc burning inside a cylindrical polytetrafluoroethylene (PTFE) tube is investigated. Finally, to investigate the effect of forced flow near CZ, a self-blast arrangement is adopted with a heating volume attached to the PTFE tube. The test circuit can generate a current of 130 A at 190 Hz. To investigate the interruption performance, the IRRRV is varied from 9.8 V/ $\mu$ s to 84.9 V/ $\mu$ s. Mainly, three different filling pressures are tested: 1 bar (atmospheric pressure), 20 bar, and 40 bar, the latter being in the SC region. To study the effect of the SC state on the interruption performance, some tests are conducted at 30 bar (subcritical) and 35 bar filling pressure (supercritical) in the self-blast arrangement.

## 2. Experimental setup

### 2.1. Test circuit

The test setup is shown schematically in figure 1. It consists of a charging and a discharging section of a 7.2  $\mu$ F high voltage (HV) capacitor bank,  $C$ , shown in figure 1(a). The capacitor  $C$  is charged to a predefined charging voltage of 15 kV by closing the switch  $S_C$ . Once the capacitor  $C$  is fully charged,  $S_C$  is opened to disconnect the test circuit from the grid. The capacitor  $C$  is discharged by closing the switch,  $S_D$ . Once  $S_D$  is closed, current starts flowing through the inductor,  $L$ , and further through an ignition copper wire inside an arcing chamber. Once the switch  $S_D$  is closed, it remains in closed position until the test is over.

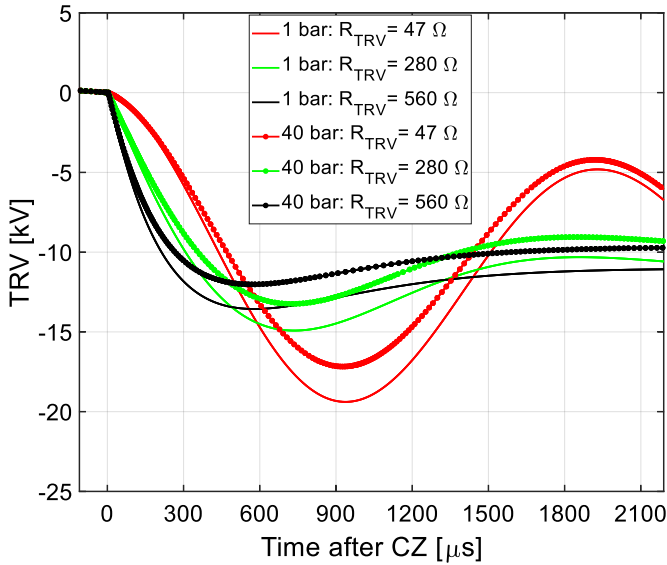


**Figure 2.** Influence of the arc voltage on the TRV shapes for different  $R_{TRV}$  s.

A pressure tank of 15.7-liters rated for 500 bar is used as an arcing chamber, shown schematically in figure 1(b). A 24-kV miniature HV cable is fed through the flange of the pressure tank and held in position by several insulating supports. The ignition wire is mounted on two arc-resistant copper-tungsten (Cu-W) electrodes which are kept at a fixed distance of 50 mm. Once the current starts flowing, the ignition wire melts due to adiabatic heating and initiates the arc. The current continues to flow until CZ where the current is momentarily interrupted. A controlled voltage stress across the electrodes is applied after CZ. The TRV shaping capacitor,  $C_{TRV}$  is kept fixed at 1.2  $\mu\text{F}$ . By changing the resistance  $R_{TRV}$ , the IRRRV is varied [18]. In this paper, the IRRRV is defined as the rate of change of TRV from CZ up to 50  $\mu\text{s}$  after CZ. As the arc resistance varies with the filling pressure and the type of the arc (free-burning or tube constricted), the amplitude of the arc current also changes. The arc-current amplitude varies from 130 A for the minimum arc voltage (free-burning, 1 bar) to 120 A for the maximum arc voltage (self-blast, 40 bar). One possible solution to overcome the challenge of slightly different arc current amplitudes would be to increase the charging voltage of the capacitor. However, changing the charging voltage would also influence the stored energy of the capacitor and the IRRRV. Hence, in this paper, the charging voltage of the capacitor is kept constant while the slight change of the arc current amplitude is considered as the property of different types of arc.

The arc resistance also plays a role in the shape of the TRV. The rate of rise of recovery voltage (RRRV) is defined as the rate of change of 20% of the  $TRV_{peak}$  to 80% of the  $TRV_{peak}$  [19]. The IRRRV is less influenced by the arc resistance. The circuit is simulated in MATLAB Simulink to calculate the current amplitude, IRRRV, RRRV,  $TRV_{peak}$  and time to  $TRV_{peak}$  from CZ. The TRV shape is first simulated considering the arc voltages for different test cases. A test case is defined as the tests performed at a particular nozzle arrangement,

filling pressure, and IRRRV value. The simulated TRV as a function of three different  $R_{TRV}$  for two different filling pressures is plotted in figure 2. It can be seen that the TRV amplitude is highest when  $R_{TRV}$  is lowest. The TRV peak gradually decreases as  $R_{TRV}$  increases. The filling pressure, on the other hand, reduces the TRV peak due to the high arc voltage. The voltage measurement in the existing setup saturates above 5 kV. All the simulated TRV shapes are matched with the measured TRV to calculate the IRRRV, RRRV,  $TRV_{peak}$  and the time to  $TRV_{peak}$  from CZ. The circuit parameter and the respective TRV parameters for all the test cases are presented in table 1.

## 2.2. Test object

Three different contact and nozzle configurations are tested, as shown in figure 3. In the first design, the arc burns freely between two fixed electrodes (a ring and a pin electrode) kept at 50 mm apart without any forced gas flow. The electrode tips are made of arc resistant copper tungsten (Cu-W). An arc in this configuration is termed as free-burning. Some of the results from the thermal interruption performance of free-burning arcs in ultrahigh-pressure  $N_2$  have been reported in a recent conference publication [20].

In the second configuration, a PTFE tube with inner diameter of 4 mm is mounted on the ring electrode, as shown in figure 3(b). Based on the Lowke's theory of free-burning arc, the arc radius at different filling pressures were calculated and reported in an earlier publication [14]. The free-burning arc diameter for the current of 150 A was calculated to be 8 mm, 3 mm, and 2.7 mm at 1 bar, 20 bar and 40 bar, respectively [14]. If the inner diameter of the tube is too large compared to the arc diameter, this reduces the interaction between the arc and the tube. Whereas, if the tube diameter is too small, it affects the flow of gas inside the tube. In this study, 4 mm tube diameter is considered which ensures the interaction of the arc and the tube without affecting the gas flow severely as the current interruption is considered as the objective in this study. The ignition wire is passed through the PTFE tube and attached to the electrodes. Afterward, the pin electrode is pushed inside the tube to allow the ablated gas to flow out of the tube through the ring electrode outlet only. The interelectrode gap is kept fixed at 50 mm.

In the final configuration, a heating volume of 3.17  $\text{cm}^3$  is attached behind the ring electrode (termed as self-blast arrangement), as shown in figure 3(c). Two holes (diameter = 3 mm) in the middle of the interelectrode gap act as vents. During the high-current phase, some of the ablated fluid leaves through the vents while the rest is stored in the heating volume. At CZ, the over-pressure built up in the heating volume generates a backflow of relatively cold fluid from the heating volume and through the vent to cool the arc. The interelectrode gap is kept fixed at 50 mm, as seen in figure 3(c). When a PTFE tube is used (tube and self-blast arrangement), the PTFE tube is changed after ten tests.

**Table 1.** Circuit parameter and calculated IRRRV, RRRV, TRV<sub>peak</sub> an time to TRV<sub>peak</sub> from CZ for different test cases.

Pressure (bar)	R <sub>TRV</sub> (Ω)	IRRRV (V/μs)	RRRV (V/μs)	TRV <sub>peak</sub> (kV)	Time to TRV peak from CZ (μs)
01	47	9.8	33.8	22.1	890
	140	22.4	30.9	19.3	842
	280	43.0	32.9	17.0	720
	420	63.9	39.9	15.9	628
	560	84.8	46.6	15.4	542
20	47	9.8	30.9	20	880
	140	22.4	28.1	17.4	810
	280	43.0	31.3	15.2	704
	420	63.9	38.1	15.1	620
	560	84.8	43.3	14.5	530
40	47	9.8	29.6	17.3	770
	140	22.4	24.4	14.2	790
	280	43.0	31.0	14.9	680
	420	63.9	37.0	14.3	616
	560	84.8	39.6	13.3	510

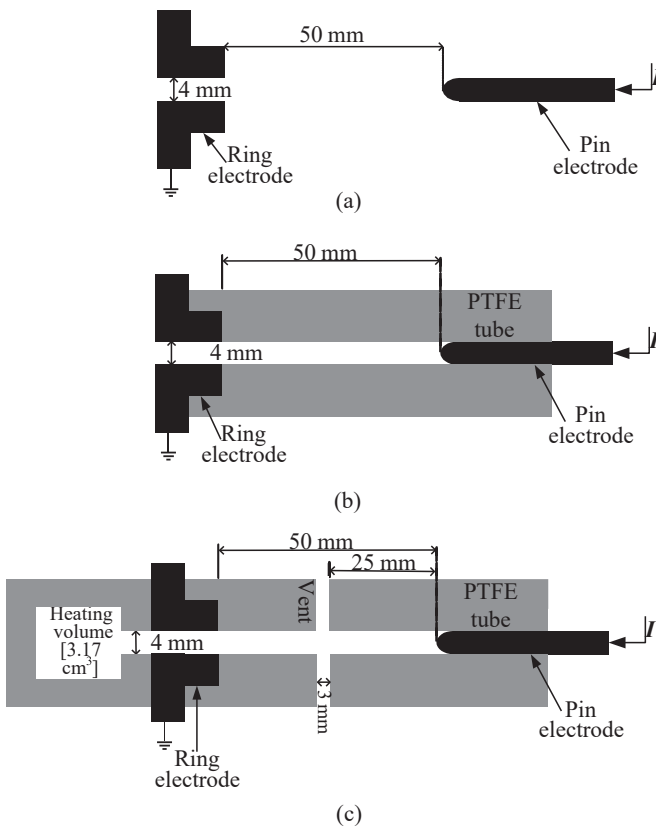


**Figure 3.** Electrode setup and nozzle arrangement, (a) free-burning arc, (b) tube constricted arc (without heating volume), (c) self-blast arrangement (with heating volume).

**2.3. Measured parameters**

Two HV probes with different voltage ranges are used to measure the arc voltage and the TRV across the electrodes. The HV probes are connected to the current path before and after the pressure tank, as shown in figure 1(a). A shunt resistor is used to measure the arc current. Moreover, a post-arc current sensor is used to measure the small currents near CZ. The

post-arc current sensor is essentially a clamped resistive shunt with antiparallel diodes [21]. The diodes bypass the resistor shunt when the current is high. When the current is low, and thus, the voltage is lower than the diodes’ forward voltage, all current flows through the resistor shunt. Both current sensors are connected on the high voltage side of the arcing chamber on a floating potential, see figure 1(a). All the data is sent to the control room via optical fiber links and recorded in a digital oscilloscope for further analysis. The sampling rate is 10 MHz.

Two different kinds of pressure measurements are carried out. One is the static pressure or the filling pressure of the pressure vessel and the other is the dynamic pressure rise in the heating volume of the self-blast arrangement. The filling pressure is measured with a static pressure sensor. The static pressure of the pressure vessel increases when N<sub>2</sub> from the gas bottle enters in the pressure tank through the valve. Once the desired filling pressure is reached, the valve is closed. For dynamic pressure inside the tank, a piezoelectric sensor is placed inside the tank and the electrical signals from sensor are taken out of the tank through signal penetrator. For dynamic pressure measurements, only few tests are carried which is reported elsewhere [22].

In the free-burning arc and tube-constricted arc configurations, ten tests are conducted for all three pressure levels at IRRRV of 9.8 V/μs. For the rest of the IRRRV values, at least five tests are performed for each filling pressure. In total, 90 tests are conducted for both the free-burning arc and tube constricted arc arrangement. For the self-blast arrangement, ten tests are conducted for IRRRV of 43.0 V/μs at 1 bar, 20 bar, 30 bar, 35 bar, and 40 bar. For the rest of the R<sub>TRV</sub> settings, five tests are conducted at 1 bar, 20 bar, and 40 bar filling pressures. In total, 110 tests are carried out using the self-blast arrangement.

**2.4. Procedure**

For all R<sub>TRV</sub> settings, experiments at three different filling pressures are conducted: 1, 20 and 40 bar. Additionally, for

the self-blast arrangement and the  $R_{TRV}$  giving an IRRRV of  $43 \text{ V}/\mu\text{s}$ , experiments are also conducted at 30 bar (subcritical) and 35 bar (supercritical)  $\text{N}_2$ . Before each test, the ignition wire is mounted by hand and the pressure vessel is closed. Afterward, the pressure vessel is flushed and then filled with industrial-grade  $\text{N}_2$  to ensure more than 99% pure  $\text{N}_2$  inside the pressure tank. After the test, the procedure is repeated. The gas handling and the circuit are remotely controlled from a separate room located at a safe distance.

### 3. Experimental results

A typical measurement of the arc voltage and the arc current during a test is shown in figure 4. The voltage peak at approximately 0.2 ms marks the melting of the copper wire and initiation of the arc. Due to the high voltage rise during the melting of the copper wire, some of the energy in capacitor  $C$  goes to charge the TRV shaping capacitor,  $C_{TRV}$ . Such a case of charging the TRV shaping capacitor can be seen in figure 4 by the collapse of the arc current during the melting of the ignition wire at approximately 0.2 ms. The current continues to flow in the ignited arc until CZ (at approximately 2.6 ms), where the current is momentarily interrupted. The temperature of the arc can not change instantaneously. As a result, some charge carriers are still present in the post-arc channel. Just after CZ, these remaining charge carriers are accelerated by the transient recovery voltage stress. Such a movement of charge carriers after CZ is often observed as a post-arc current. If the post-arc current is high enough, sufficient energy may deposit in the post-arc current column to re-establish the arc, seen as re-ignition in figure 4. The re-ignition is marked by the collapse of the TRV and by the sudden increase of the arc current. The re-ignition shown in figure 4 is due to the thermal failure. Thermal re-ignitions are initiated by the presence of high post-arc current whereas the dielectric restrikes are caused mainly due to the low dielectric strength compared to TRV. The dielectric restrike occurs typically after several hundred of microseconds and when the TRV is very high. The dielectric restrikes are also considered when the interruption performance is analyzed. In this paper, the time between CZ and the re-ignition caused by thermal or dielectric failure is defined as the time to re-ignition ( $\Delta t$ ).

#### 3.1. Interruption performance

Table 2 lists the number of successful current interruptions compared to the number of tests conducted. The successful interruption means when the current is interrupted at the first natural CZ, i.e. after first half cycle. The arcing time in the first half cycle is fixed and is equal to approximately 2.4 ms. First, for the free-burning arc configuration, among the 90 tests conducted at different IRRRVs, no successful current interruptions were observed.

For tube-constricted arcs, at all pressure levels, when the IRRRV was higher than  $9.8 \text{ V}/\mu\text{s}$ , no successful current interruption was recorded. However, at  $9.8 \text{ V}/\mu\text{s}$ , the arc was interrupted five times at 1 bar, 0 times at 20 bar and 10 times at 40 bar out of the 10 tests conducted at each filling pressure.

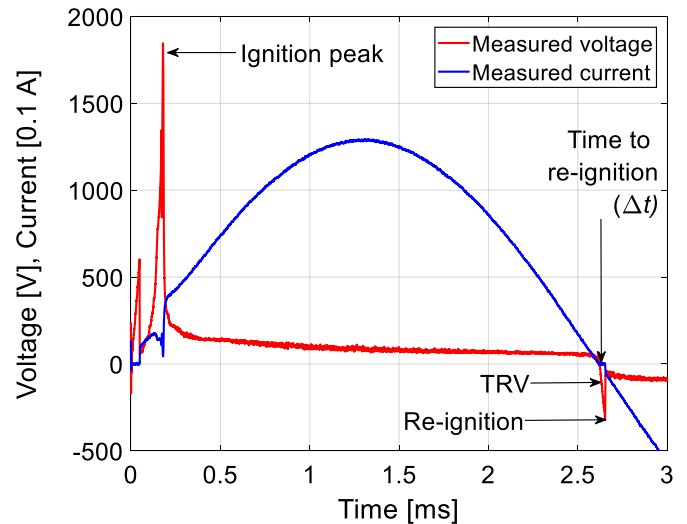


**Figure 4.** Measured arc voltage and arc current for atmospheric pressure nitrogen arc with an arc peak current of 130 A and an IRRRV of  $9.8 \text{ V}/\mu\text{s}$ .

The number of successful interruptions compared to the number of tests conducted is highest for the self-blast arrangement. In this arrangement, at 1 bar filling pressure, the percentage of successful interruptions is found to be 40%–60% depending on the IRRRV. At 20 bar filling pressure, the percentage of successful interruptions is found to be 100% when the IRRRV is  $9.8 \text{ V}/\mu\text{s}$ , decreasing to 20% or lower when the IRRRV is higher. At 40 bar filling pressure, the ratio of successful interruptions is 100% when the IRRRV is  $22.3 \text{ V}/\mu\text{s}$  or less. The ratio of successful interruptions went to 40% for IRRRVs of  $63 \text{ V}/\mu\text{s}$  and  $84.8 \text{ V}/\mu\text{s}$ . No change in current interruption performance is observed when transitioning from gas to the SC state. For both the 30 bar (subcritical) and 35 bar (supercritical) filling pressure, the percentage of successful interruption was measured to be 50%. It is observed that the interruption performance at 40 bar filling pressure is better than at atmospheric pressure when the IRRRV is  $22.3 \text{ V}/\mu\text{s}$  or less. Moreover, at 20 bar filling pressure, the interruption performance is better than at atmospheric pressure only when the IRRRV is  $9.8 \text{ V}/\mu\text{s}$ .

#### 3.2. Time to re-ignition

The time to re-ignition ( $\Delta t$ ) as a function of IRRRV for different filling pressures is plotted in figure 5. The free-burning arc configuration is presented in figure 5(a). Each data point represents the average of ten ( $\text{IRRRV} = 9.8 \text{ V}/\mu\text{s}$ ) or five tests ( $\text{IRRRV} \neq 9.8 \text{ V}/\mu\text{s}$ ). The error bar corresponds to the highest and lowest measured values of  $\Delta t$ . For an IRRRV of  $9.8 \text{ V}/\mu\text{s}$ , the average time to re-ignition at 1 bar is approximately  $35 \mu\text{s}$ . The re-ignition time goes down to approximately  $13 \mu\text{s}$  when the filling pressure is 20 bar or 40 bar. A shorter time to re-ignition at high filling pressures (20 bar or 40 bar) compared to 1 bar is observed for all the measured IRRRV values. The difference in time to re-ignition for arcs burning in 20 bar and 40 bar  $\text{N}_2$  is less prominent.

**Table 2.** Number of successful current interruptions compared to the number of tests conducted at different IRRRVs for different filling pressures and test arrangements.

Test arrangement	Filling pressure (bar)	Number of successful interruptions / the number of tests conducted				
		IRRRV 9.8 V/μs	IRRRV 22.4 V/μs	IRRRV 43 V/μs	IRRRV 63.9 V/μs	IRRRV 84.8 V/μs
Free burning	1	0/10	0/5	0/5	0/5	0/5
	20	0/10	0/5	0/5	0/5	0/5
	40	0/10	0/5	0/5	0/5	0/5
Tube constricted	1	5/10	0/5	0/5	0/5	0/5
	20	0/10	0/5	0/5	0/5	0/5
	40	10/10	0/5	0/5	0/5	0/5
Self-blast (with a heating volume)	1	3/5	2/5	6/10	3/5	2/5
	20	5/5	1/5	1/10	1/5	1/5
	40	5/5	5/5	6/10	2/5	2/5
	30	-	-	5/10	-	-
	35	-	-	5/10	-	-

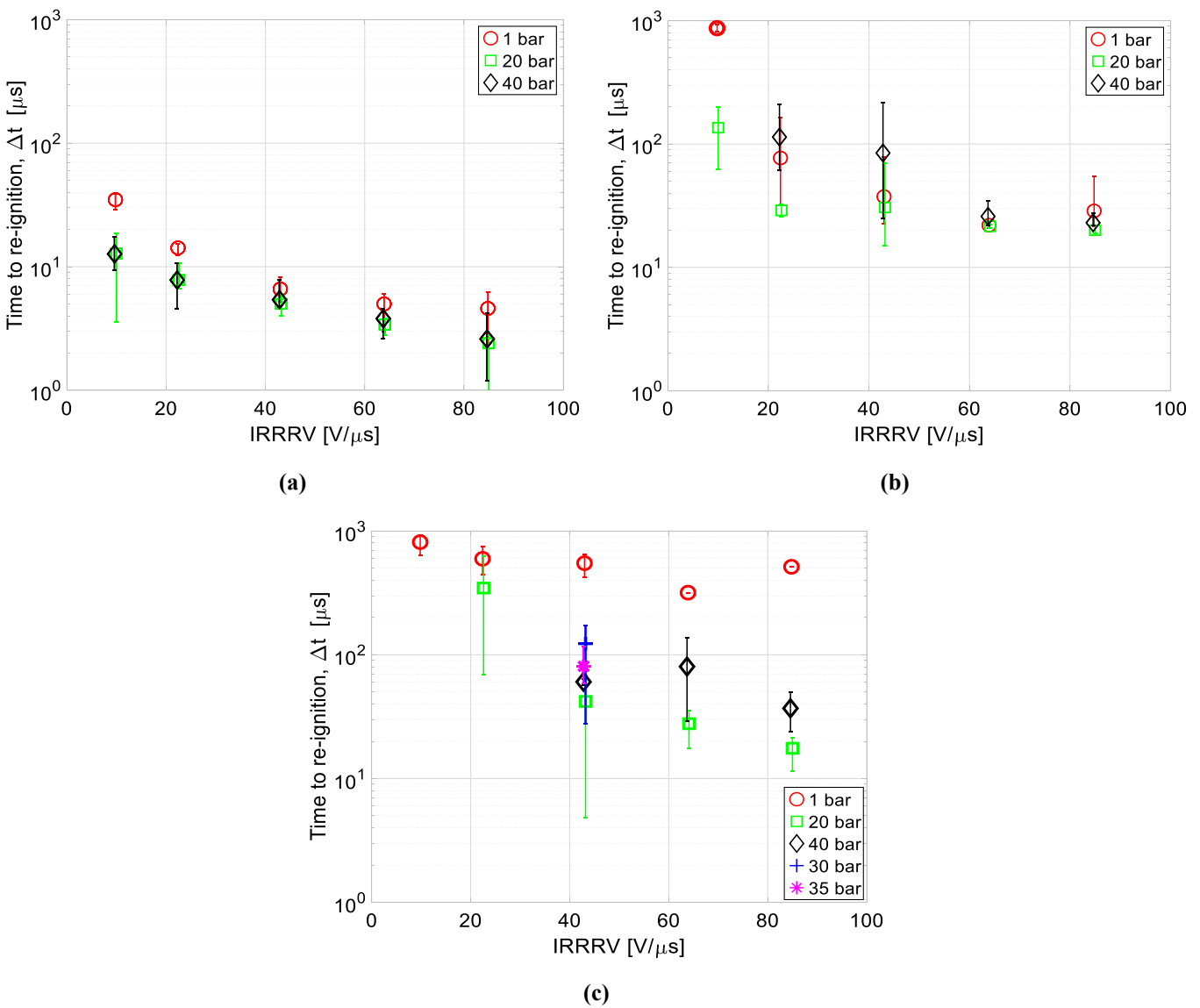


**Figure 5.** Re-ignition time as a function of IRRRV for different filling pressures and at different electrode and nozzle configurations. (a) Free-burning arc. (b) Tube constricted arc. (c) Self-blast arrangement.

The times to re-ignition for the tube-constricted arc at different filling pressures are shown in figure 5(b). Similar to the free-burning arc arrangement, in the tube-constricted arc configuration, the time to re-ignition is observed to decrease as the IRRRV increases. However, compared to free-burning arcs, the time to re-ignition is significantly longer for all filling pressures when the arc burns inside a PTFE tube. The average time to re-ignition at atmospheric pressure with an IRRRV of 9.8 V/ $\mu$ s increases from 35  $\mu$ s to 955  $\mu$ s. Moreover, at 1 bar and with IRRRV of 9.8 V/ $\mu$ s, 5 out of 10 tests were successful interruptions. The average of the 5 failed cases at 1 bar pressure with an IRRRV = 9.8 V/ $\mu$ s is shown in figure 5(b). For all successful interruptions in a test case, no data point is shown, as the case of 40 bar filling pressure at an IRRRV of 9.8 V/ $\mu$ s. It is observed that in tube-constricted configuration, at 40 bar filling pressure, the time to re-ignition is slightly longer compared to the tests at 1 bar.

For the self-blast arrangement, the average time to re-ignition as a function of the IRRRV is plotted in figure 5(c). At 40 bar filling pressure, 5 successful interruptions are recorded out of 5 tests performed for both the IRRRV of 9.8 and 22.4 V/ $\mu$ s, whereas at 20 bar filling pressure 5 successful interruptions are recorded out of 5 tests performed for an IRRRV of 9.8 V/ $\mu$ s. Hence, these data points are not shown in figure 5(c). At 1 bar filling pressure, the average time to re-ignition among the failed interruptions are observed to be more than 300  $\mu$ s. In general, the time to re-ignition is found to be the longest for the self-blast arrangement among all three electrode and nozzle arrangements. The time to re-ignition in the self-blast arrangement is also found to decrease with the increase of the IRRRV, as expected. In the self-blast arrangement, apart from when IRRRV is 9.8 V/ $\mu$ s, the re-ignition happens faster for 20 bar filling pressure compared to 1 bar and 40 bar. No significant change in time to re-ignition is observed between 30 bar (subcritical) and 35 bar (supercritical) filling pressure (IRRRV = 43 V/ $\mu$ s).

### 3.3. Breakdown voltage

The breakdown voltage as a function of filling pressure for different IRRRVs at different electrode and nozzle configurations is shown in figure 6. In free-burning arrangement, the breakdown voltage is less dependent on the IRRRVs for all filling pressures. The breakdown voltages at a higher filling pressure (e.g. 20 bar, 40 bar) is observed to be lower than at 1 bar. In tube-constricted arrangement, the breakdown voltage at 1 bar for the IRRRV of 9.8 V/ $\mu$ s is observed to be approximately 19 kV, which is a dielectric failure. For the rest of the cases, the breakdown voltage is less than 2.5 kV and are of thermal failures. In the self-blast arrangement, the breakdown voltages at 1 bar are found highest for all three filling pressures. At 20 bar filling pressure, when the IRRRV is 22.4 V/ $\mu$ s, the average breakdown voltage is approximately 7.2 kV. Whereas, for the IRRRV of 43 V/ $\mu$ s and higher, the breakdown voltage is observed to be less than 4 kV for 20 bar and 40 bar filling pressures.

### 3.4. Post-arc Current

A comparison of the average post-arc current in the free-burning, tube-constricted and the self-blast type arrangements as a function of filling pressure for different IRRRV is plotted in figure 7. Each data point represents the average of the experiments conducted in that test case. The post-arc current measurement saturates at 1000 mA. For all cases, a post-arc current higher than 1000 mA leads to failed interruption. In the case, when there are some successful and some failed interruptions, a filled marker represents the average of the successful current interruptions. Whereas, an empty marker represents the average of the failed interruptions for any particular test case, see figure 7(d).

First, the post-arc current of the free-burning arc as a function of different IRRRV is plotted in figures 7(a)–(c). It can be observed that the post-arc current increases with the increase of the IRRRV, see 10  $\mu$ s after CZ in figures 7(a)–(c), which is expected. When compared with different filling pressures, for any particular IRRRV, the average post-arc current at 20 bar and 40 bar is higher than at atmospheric pressure, see up to time of re-ignition in figures 7(a)–(c). No significant difference in post-arc current is observed between 20 bar and 40 bar filling pressure for different IRRRVs. From figures 7(a)–(c) it can be seen that the re-ignition happens faster at higher filling pressures in comparison to the atmospheric pressure.

The post-arc current for tube-constricted arcs at different filling pressures and IRRRVs is shown in figures 7(d)–(f). At the lowest IRRRV of 9.8 V/ $\mu$ s, the post-arc current at 1 bar is observed to be the lowest among all the filling pressures, see figure 7(d). The failed interruption at 1 bar is probably a dielectric restrike (approximately 1 ms after CZ). Hence, no significant change in post-arc current is observed between successful and failed tests at 1 bar, see figure 7(d). The high post-arc current at 40 bar flows for a relatively long time (approximately 1500  $\mu$ s) and gradually diminishes. No re-ignition is observed for 40 bar filling pressure when the arc burns inside a PTFE tube for an IRRRV of 9.8 V/ $\mu$ s. However, at 20 bar filling pressure, all the experiments conducted with an IRRRV of 9.8 V/ $\mu$ s resulted in a re-ignition, see figure 7(d). The post-arc current measured for 20 bar filling pressure is found to be the highest for different IRRRV settings when the arc burns inside the PTFE tube. In general, the post-arc current increases as the IRRRV increases, see figures 7(d)–(f), which is expected.

The average post-arc current measured for the self-blast arrangement at different filling pressures and IRRRVs is shown in figures 7(g)–(i). For the lowest IRRRV setting of 9.8 V/ $\mu$ s, the self-blast arrangement shows significantly lower post-arc currents compared to the free-burning and tube-constricted arrangements, see figure 7(g). All the experiments conducted with the self-blast arrangement, at 20 bar and 40 bar filling pressure were successful current interruptions at the lowest IRRRV. When the IRRRV was increased to 22.3 V/ $\mu$ s, the post-arc currents at 1 bar and 40 bar were still found to be low. In contrast, a significantly higher post-arc current is recorded for 20 bar. At an IRRRV of 43 V/ $\mu$ s, the post-arc current again increases for higher filling pressures (20 bar and 40 bar) compared to at atmospheric pressure arc.

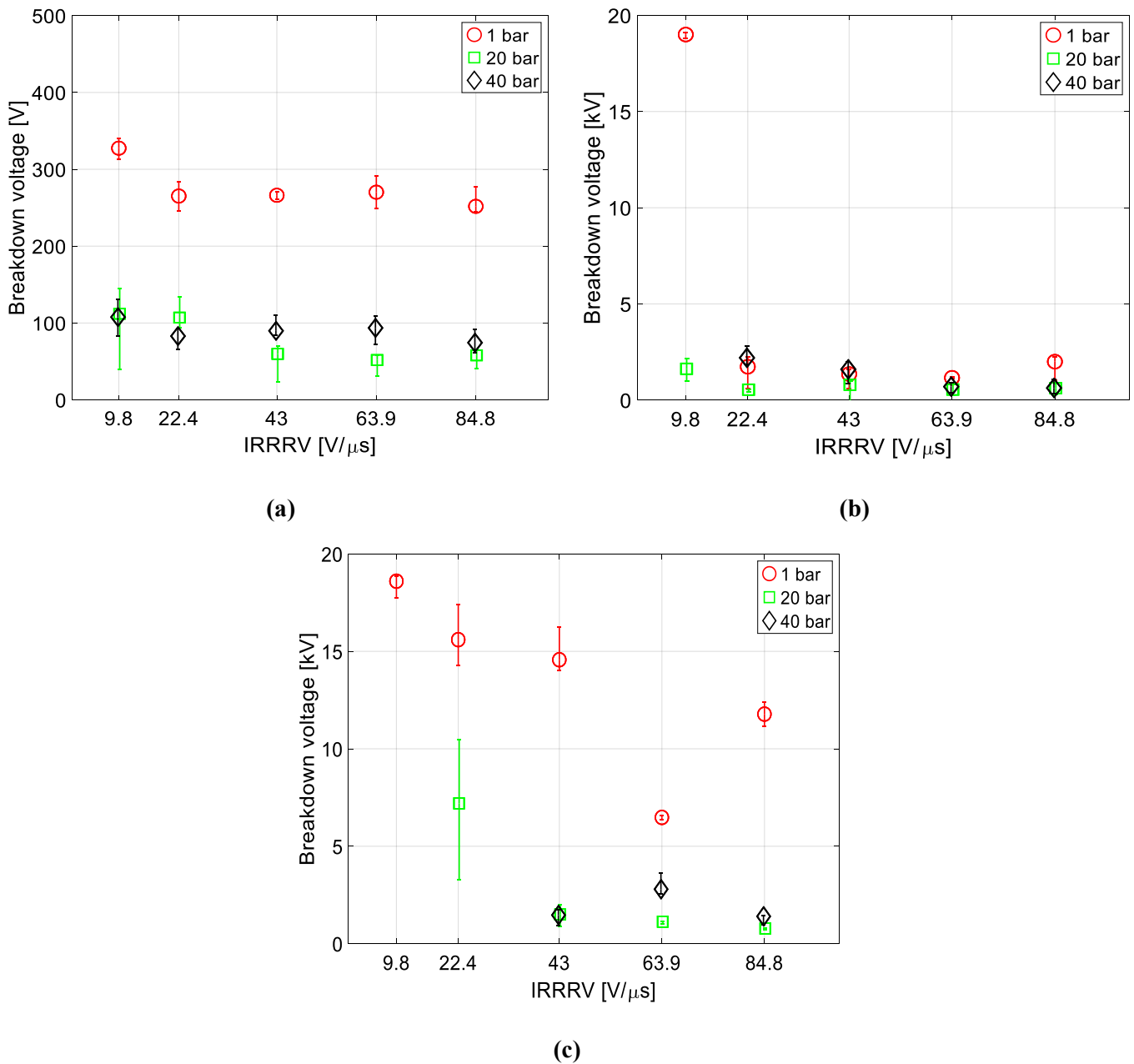


**Figure 6.** Breakdown voltage as a function of IRRRV for different filling pressures and at different electrode and nozzle configurations. (a) Free-burning arc. (b) Tube-constricted arc. (c) Self-blast arrangement. The scale of the Y axis is not same for three different configurations.

The post-arc current for the self-blast arrangement at different IRRRVs for 40 bar is shown in figure 8. At IRRRVs of 9.8 V/μs and 22.3 V/μs, the measured post-arc current is low. At an IRRRV of 43 V/μs, the measured post-arc current is more than 100 mA, but still, the current is successfully interrupted. However, at IRRRVs of 63.9 V/μs and 84.8 V/μs, the post-arc current was more than 200 mA and resulted in a thermal re-ignition.

#### 4. Discussions

For the free-burning arc, the increase of the pressure inside the arc is greatest at the cathode-spot where the current density is

the highest [23]. This increase of pressure near cathode-spot induces an axial flow. For a lower current (< 30 A), however, the axial flow reduces, and the natural convection plays the dominant role. For tube-constricted arc, the inner surface of the PTFE tube ablates when the arc current is high. The intensity of the ablation reduces when the current approaches the CZ. Nonetheless, even after the arc is extinguished, the nozzle continues to ablate for a few milliseconds after CZ [24]. When a heating volume is used, in self-blast arrangement, during the high current phase, the pressure rises in the heating volume. The overpressure in the heating volume of the self-blast arrangements is measured for few tests, which are reported elsewhere [22]. The pressure rise in the heating volume is observed to increase with the filling pressure.

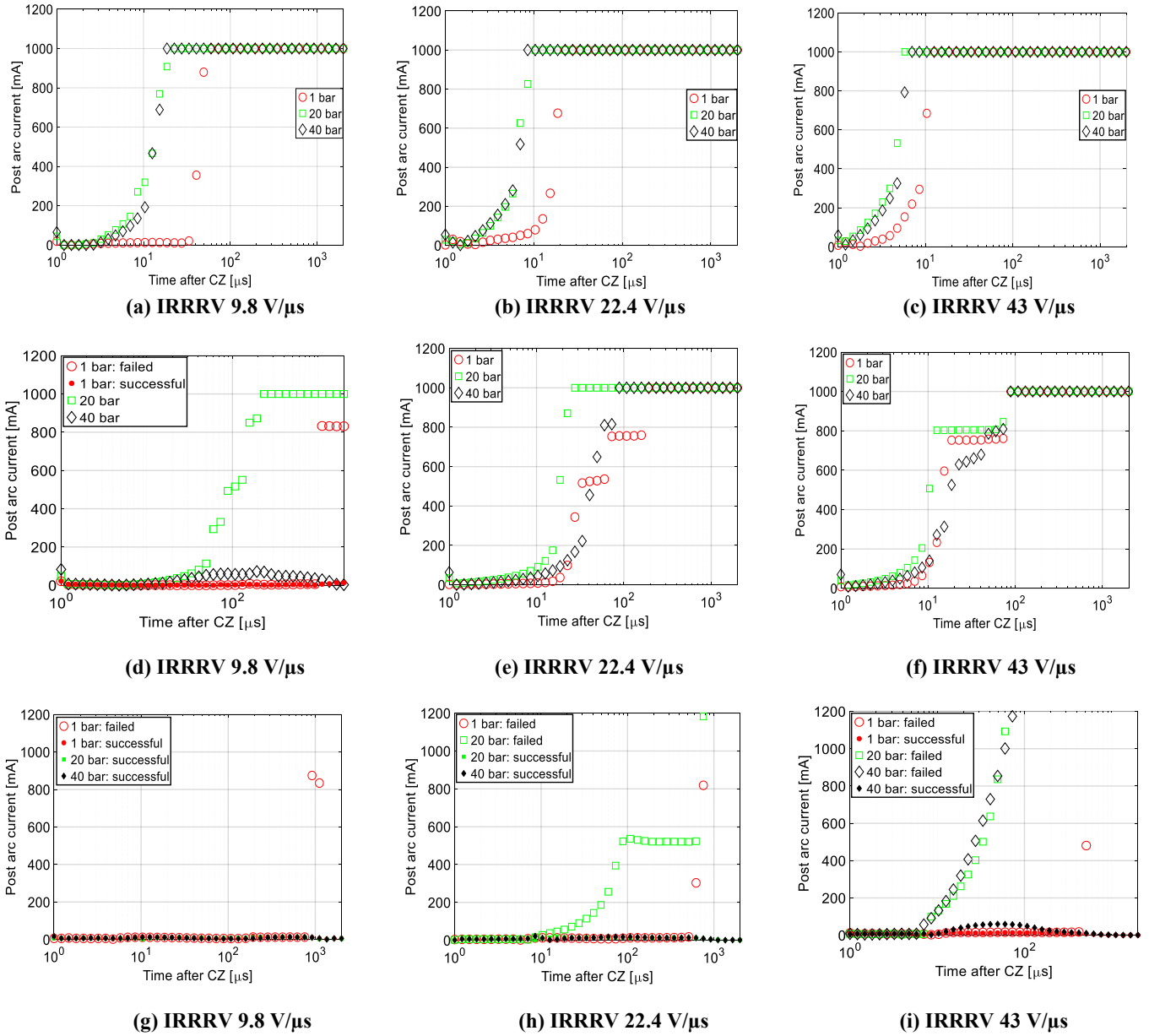


**Figure 7.** Average post-arc current for different configuration (a)–(c) free-burning, (d)–(f) tube constricted, (g)–(i) self-blast arrangement. The filled markers are for successful.

The arc current is momentarily interrupted at each CZ crossing. Just after CZ, due to the energy-storing elements (capacitors and inductors) in the circuit, voltage stress is developed across the electrodes. As the stored thermal energy of the arc channel is not dissipated instantaneously, some charge carriers may still remain in the electrode gap. These charge carriers get accelerated by the voltage difference between the electrodes and are observed as a measurable post-arc current. If the energy dissipation in the arc channel due to the post-arc current is high compared to the cooling of the medium, a thermal re-ignition may occur [15]. Under the simplifying assumption of a homogeneous post-arc channel, the post-arc current can be written as

$$I = nqvA, \tag{1}$$

where  $n$  is the number of charge carriers per volume,  $q$  is the charge,  $v$  is the velocity of the charge carriers and  $A$  is the cross-sectional area of the post-arc channel. The velocity of the charge carriers is linearly proportional to the applied voltage stress between the electrodes after CZ. As the IRRRV is increased, the rate of change of TRV increases. In other words, for a given time after CZ, the voltage stress across the electrodes is high for high IRRRV. The high electric field will accelerate the remaining charge carriers faster which would increase the post-arc current. A high post-arc current increases the energy deposition in the post-arc channel and increases the possibility of early re-ignition. This causes the time to BD to go down as the IRRRV is increased. As a result, a faster time to re-ignition is observed for all filling pressure tested when the IRRRV is increased.

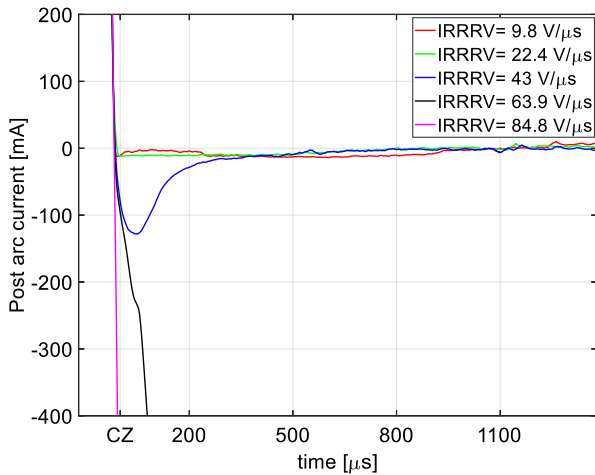


**Figure 8.** Post-arc current at 40 bar filling pressure in the self blast arrangement for different IRRRV.

When the filling pressure increases, the arc voltage rises too. Consequently, the energy dissipated in the arc channel increases with increasing filling pressure. Moreover, due to the high filling pressure the arc radius decreases [5, 13]. In the absence of forced cooling near CZ, the hot core of the arc fails to dissipate the heat quickly. The relatively high temperature of the arc core at a high filling pressure after CZ may result in a high number of charge carriers at a high filling pressure, especially when the cooling is not sufficient. The velocity of charge carriers also depends on the mobility of the charge carriers. Electrons being lighter, move faster than ions. A higher pressure, however, tends to reduce the mobility of the electrons due to its collision with neutral and charged particles [25]. The increase in temperature of the post-arc channel at a higher filling pressure may compensate for the reduced mobility of electrons caused by the high density [26]. As a result, the post-arc current may increase at a higher filling pressure and contribute to a faster re-ignition.

The thermal re-ignition characteristics of free-burning arc at 20 bar and 40 bar gas filling pressures are found to be quite similar. In previous work, for an arc peak current of 150 A at 350 Hz, the arc radius of the free-burning arc was calculated to be approximately 4 mm at atmospheric pressure [14]. In comparison, the calculated free-burning arc radius was 1.5 mm and 1.43 mm for an arc burning at 20 bar and 40 bar, respectively [14]. It was reported that the arc is constricted by filling pressure significantly at 20 bar filling pressure compared to at atmospheric pressure, whereas the constriction is not much greater when comparing an arc at 40 bar to one at 20 bar. This may explain the similarity in re-ignition properties for arcs burning at 20 bar and 40 bar filling pressure in the free-burning configuration.

When the arc burns inside the PTFE tube, the flow stagnation point lies near to the pin electrode as the pin electrode blocks any gas flow out. The axial pressure distribution in this configuration is parabolic where the maximum pressure lies at the stagnation point [27–29]. As a result, the plasma velocity reaches its maximum near the exit point through the

ring electrode. It has been observed that the time to re-ignition increases when the arc burns inside a tube in comparison to the free-burning arc, which is expected. The PTFE ablates when the arc burns inside the PTFE tube. It has been reported that even after the arc is extinguished, the nozzle continues to ablate for a few milliseconds after CZ [24]. The PTFE vapor cools the arc which may contribute to the higher time to re-ignition when the arc burns inside the tube in comparison to the free-burning arc. For the lowest IRRRV, some successful current interruption is observed when the arc burns inside the tube.

The self-blast arrangement shows the best interruption performance among the three different arrangements investigated. The interruption performance improves at high filling pressure when the IRRRV is lowest in the self-blast arrangement. As the filling pressure increases, the density of the gas increases too. Under forced gas flow, due to the high density, the cooling is enhanced at a high-filling pressure. As a result, the post-arc current recorded is low and the interruption performance improves in the self-blast arrangement at lower IRRRV settings. However, when the IRRRV is high, the post-arc current increases rapidly which may initiate a thermal re-ignition. In self-blast arrangement, at 1 bar filling pressure, the percentage of successful interruption is less dependent on the IRRRV. The IRRRV plays an important role in the post-arc current and the thermal failures. However, the failures at 1 bar are of dielectric nature, as can be seen from the high breakdown voltage, see figure 6(c).

For the tube constricted and the self-blast arrangements, it is observed that the interruption performance is better at 40 bar than at 20 bar filling pressure. However, in the free-burning arc, the re-ignition time for 20 bar and 40 bar filling pressure was observed to be similar. The arc temperature near CZ varies at different filling pressures at different electrodes and nozzle arrangements. High filling pressure changes the material properties of the plasma. However, the material properties of the  $N_2$  plasma in the range of up to several tens of bars is not available in the literature. As a result, the physical property variations of the high pressure air plasma is summarized and shown in table 3 [30, 31]. As the pressure is increased, the thermal conductivity peak of air shifts with the filling pressure. If the temperature of the arc just after CZ is such that the thermal conductivity is low, then the cooling will be affected. Moreover, increasing the pressure also increases the viscosity, which may shift the flow characteristics from being turbulent to more laminar, thus affecting the cooling. The reduced thermal conductivity together with increasing viscosity may inversely affect the interruption performance at 20 bar filling pressure.

Almost identical current interruption characteristics are observed when the filling pressure is 30 bar (subcritical) and 35 bar (supercritical). Previously, it has been reported that the arc voltage does not change abruptly during the transition from gas to the SC state in  $N_2$  [12]. The physical properties such as electrical conductivity, viscosity, thermal conductivity do not change abruptly for  $N_2$  during the transition from gas to the SC state [31]. The effect of SC state on the interruption performance is not observed.

**Table 3.** Effect of filling pressure on different parameters influencing the current interruption.

Parameters	Effect of pressure
Arc radius	Decreases non linearly.
Thermal conductivity	Increases with pressure after 18 000 K. Shift of the thermal conductivity peak towards high temperature before 18 000 K.
Viscosity	Increases with pressure. The viscosity peak as a function of temperature shifts towards high temperature.
Electrical conductivity	Increases with pressure after 15 000 K, decreases with pressure for temperature less than 15 000 K.
Energy density of the arc	Increases with pressure.

Among the failed current interruptions at high filling pressures (e.g. 20 bar, 40 bar), thermal re-ignition is observed to be the dominant failure mechanism. In the absence of forced cooling, the temperature decay rate in the post-arc channel may get affected by the high filling pressure. It has been observed that the post-arc dielectric strength increases rapidly with the increase of high filling pressure [32]. In the free-burning arc arrangement, just after CZ up to a critical time instants, the dielectric strength is observed to be low even at a high filling pressure [32]. As a result, if the cooling of the arc channel is not sufficient, a high filling pressure may result in higher post-arc current and in a subsequent thermal re-ignition. However, if the thermal phase is successfully passed, the temperature of the post-arc channel decreases below a critical value. The increased dielectric strength with the increase of filling pressure at a relatively low temperature helps to successfully pass the dielectric phase. As a result, all the failures at high filling pressure are observed as a thermal re-ignition type in this study. At 1 bar, however, both the dielectric restrike and thermal re-ignition type of failures are observed. Hence, the thermal phase seems to be the critical phase for the current interruption in ultra-high pressure N<sub>2</sub>.

## 5. Conclusions

The current interruption performance of ultrahigh-pressure N<sub>2</sub>, with or without forced gas flow, is reported in this paper. As the filling pressure increases, the arc voltage increases too. A comparison between different kinds of arcs (free-burning, tube constricted and self-blast type) at different filling pressure is inherently difficult as the arc voltage influences the amplitude of the arc current and the TRV. Nevertheless, based on the experimental investigation, some key conclusions are drawn from the study:

- In the absence of forced gas flow, the interruption performance deteriorates with increasing filling pressure.
- A high post-arc current is observed when the arc burns at higher filling pressures (i.e. 20 bar, 40 bar) compared to at atmospheric pressure. High post-arc current leads to thermal re-ignition when cooling is not sufficient.
- Forced gas flow improves interruption performance at all filling pressures. The improved cooling at high filling pressures reduces the post-arc current when the IRRRV is low. As a result, the interruption performance improves with the forced flow at high filling pressures for low IRRRV.
- For tube constricted and self-blast arrangements, current interruption performance at 20 bar is observed to be worse than that at 1 bar, whereas 40 bar shows the best performance. The temperature-dependent thermal conductivity at different filling pressures may affect the current interruption performance. A shift in the arc temperature near CZ due to the filling pressure may result in poor cooling if the thermal conductivity is low at that arc temperature.
- Among the failed interruptions, thermal re-ignition is observed to be the dominant failure mechanism at high filling pressures.
- No obvious improvement in interruption performance is observed when N<sub>2</sub> enters the supercritical region.

## Acknowledgements

This work is supported by the Norwegian Research Council.

## ORCID iD

Fahim Abid  <https://orcid.org/0000-0001-8570-491X>

## References

- [1] Hazel T, Baerd H H, Legeay J J and Bremnes J J 2013 Taking power distribution under the sea: design manufacture and assembly of a subsea electrical distribution system *IEEE Ind. Appl. Mag.* **19** 58–67
- [2] Nordrum A ABB siemens test subsea power grids for underwater factories—IEEE spectrum. (<https://spectrum.ieee.org/energy/fossil-fuels/abb-siemens-test-subsea-power-grids-for-underwater-factories>) (Accessed: 27 September 2019)
- [3] Zhang J 2015 Supercritical fluids for high power switching PhD dissertation Department of Electrical Engineering (Netherlands: Eindhoven University of Technology)
- [4] Zhang J et al 2015 Breakdown strength and dielectric recovery in a high pressure supercritical nitrogen switch *IEEE Trans. Dielectr. Electr. Insul.* **22** 1823–32
- [5] Schmidt H P and Speckhofer G 1996 Experimental and theoretical investigation of high-pressure arcs. I: the cylindrical arc column (two-dimensional modeling) *IEEE Trans. Plasma Sci.* **24** 1229–38
- [6] Speckhofer G and Schmidt H-P 1996 Experimental and theoretical investigation of high-pressure arcs. II. The magnetically deflected arc (three-dimensional modeling) *IEEE Trans. Plasma Sci.* **24** 1239–48
- [7] Tanoue H et al 2013 Shock wave generated by negative pulsed discharge in supercritical carbon dioxide in 2013 19th IEEE Pulsed Power Conf. (PPC) pp 1–5
- [8] Tanoue H, Furusato T, Takahashi K, Hosseini S H R, Katsuki S and Akiyama H 2014 Characteristics of shock waves generated by a negative pulsed discharge in supercritical carbon dioxide *IEEE Trans. Plasma Sci.* **42** 3258–63
- [9] Zhang J, van Heesch B, Beckers F, Huiskamp T and Pemen G 2014 Breakdown voltage and recovery rate estimation of a

- supercritical nitrogen plasma switch *IEEE Trans. Plasma Sci.* **42** 376–83
- [10] Ito T and Terashima K 2002 Generation of micrometer-scale discharge in a supercritical fluid environment *Appl. Phys. Lett.* **80** 2854–6
- [11] Lock E H, Saveliev A V and Kennedy L A 2009 Influence of electrode characteristics on dc point-to-plane breakdown in high-pressure gaseous and supercritical carbon dioxide *IEEE Trans. Plasma Sci.* **37** 1078–83
- [12] Abid F, Niayesh K, Jonsson E, Stoa-Aanensen N S and Runde M 2018 Arc voltage characteristics in ultrahigh-pressure nitrogen including supercritical region *IEEE Trans. Plasma Sci.* **46** 187–93
- [13] Okuma T et al 2018 Effects of working pressure on temperature characteristics in multiphase AC arc *J. Fluid Sci. Technol.* **13** JFST0024–JFST0024
- [14] Abid F, Niayesh K and Stoa-Aanensen N S 2019 Ultrahigh-pressure nitrogen arcs burning inside cylindrical tubes *IEEE Trans. Plasma Sci.* **47** 754–61
- [15] Niayesh K and Runde M 2017 *Power Switching Components* (Gwerbestrasse: Springer)
- [16] Edels H and Ettinger Y 1962 Arc interruption and thermal reignition *Proc. IEE Part A Power Eng.* **109** 89
- [17] Garzon R D *High Voltage Circuit Breakers: design and Applications* R D Garzon (New York: Marcel Dekker)
- [18] Karimi A and Niayesh K 2009 A simple evaluation method of the thermal interruption limit of power circuit breakers *Electr. Eng.* **90** 523–8
- [19] Flurscheim C H 1982 *Power Circuit Breaker Theory and Design* (London: IET)
- [20] Abid F, Niayesh K, Thimmappa S B, Espedal C and Støa-Aanensen N 2020 Thermal interruption performance of ultrahigh-pressure free-burning nitrogen arc *21st Int. Symp. on High Voltage Engineering (ISH)* (Berlin: Springer) pp 663–71
- [21] Barrault M, Bernard G, Maftoul J and Rowe S 1993 Post-arc current measurement down to the ten milliamperes range *IEEE Trans. Power Deliv.* **8** 1782–8
- [22] Abid F, Niayesh K and Støa-Aanensen N 2019 Nozzle wear and pressure rise in heating volume of self-blast type ultra-high pressure nitrogen arc *Plasma Phys. Technol. J.* **6** 23–26
- [23] Lowke J J 1979 Simple theory of free-burning arcs *J. Phys. D. Appl. Phys.* **12** 1873–86
- [24] Babou Y, Corfdir P and Suetterlin R-P 2019 Experimental assesment of ptfе post-arc ablation *Plasma Phys. Technol.* **6** 148–51
- [25] Chen F F 2018 Introduction to plasma physics and controlled fusion *Introduction to Plasma Physics and Controlled Fusion* (Gwerbestrasse: Springer)
- [26] Bisetti F and El Morsli M 2012 Calculation and analysis of the mobility and diffusion coefficient of thermal electrons in methane/air premixed flames *Combust. Flame* **159** 3518–21
- [27] Ruchti C B and Niemeyer L 1986 Ablation controlled arcs *IEEE Trans. Plasma Sci.* **14** 423–34
- [28] Muller L 1993 Modelling of an ablation controlled arc *J. Phys. D. Appl. Phys.* **26** 1253–9
- [29] Kovitya P and Lowke J J 1984 Theoretical predictions of ablation-stabilised arcs confined in cylindrical tubes *J. Phys. D. Appl. Phys.* **17** 1197–212
- [30] Wang C et al 2016 Thermodynamic and transport properties of real air plasma in wide range of temperature and pressure *Plasma Sci. Technol.* **18** 732
- [31] D'angola A, Colonna G, Gorse C and Capitelli M 2008 Thermodynamic and transport properties in equilibrium air plasmas in a wide pressure and temperature range *Eur. Phys. J. D* **46** 129–50
- [32] Abid F, Niayesh K and Stoa-Aanensen N 2019 Post-arc dielectric recovery characteristics of free-burning ultrahigh-pressure nitrogen arc *5th Int. Conf. on Electric Power Equipment—switching technology, ICEPE-ST 2019*